

INT. J. REMOTE SENSING, 1997, VOL. 18, NO. 12, 2657-2676

NASA/CR-97-

207391

NDB

IN-45-CR  
CWAIVED

## The potential for collocated AGLP and ERBE data for fire, smoke, and radiation budget studies

067325

S. A. CHRISTOPHER and J. CHOU

Institute of Atmospheric Sciences,  
South Dakota School of Mines & Technology, 501 East Saint Joseph Street,  
Rapid City, South Dakota 57701-3995, U.S.A.

(Received 17 June 1996; in final form 4 December 1996)

**Abstract.** One month of the Advanced Very High Resolution Radiometer (AVHRR) Global Area Coverage (GAC) Land Pathfinder (AGLP) data from September 1985 are used to examine the spatial and temporal distribution of fires over four major ecosystems in South America. The Earth Radiation Budget Experiment (ERBE) scanner data are used to examine the top of atmosphere (TOA) shortwave and longwave fluxes over smoke generated from biomass burning. The relationship between the AGLP-derived Normalized Difference Vegetation Index (NDVI) and the ERBE-estimated clear sky albedos are also examined as a function of the four ecosystems. This study shows that the grassland areas in South America have the highest number of fires for September 1985, and their corresponding NDVI values are smaller than the tropical rainforest region where the number of fires were comparatively small. Clear sky statistics accumulated during the days when smoke was not present show that clear sky albedos derived from ERBE are higher for grassland areas when compared to the tropical rainforest. The results show that the AGLP can be used to determine the spatial and temporal distribution of fires along with vegetation characteristics, while ERBE data can provide necessary information on broadband albedos and regional top of atmosphere radiative impacts of biomass burning aerosols. Since the AGLP data are available from 1981 to the present day, several climate-related issues can be addressed.

### 1. Introduction

One of the foremost objectives in the upcoming Earth Observing System (EOS) programme is to use spaceborne observations in order to understand the earth and its atmosphere as an integrated system (Asrar and Dokken 1993). With a wide variety of sensors to be launched, NASA's Mission to Planet Earth (MTPE) programme is the most ambitious project ever attempted to document and understand the physical mechanisms responsible for global climate change. With terabytes of data expected to stream from these sensors every day, there needs to be a system in place that will effectively archive and distribute the data to the research community. As a precursor to the upcoming EOS mission, the NASA/NOAA Pathfinder programme, initiated in 1990 (Maiden and Greco 1994), has produced successfully several geophysical products from existing satellite data sets. These long-term data sets will provide valuable experiences with data production, archiving, handling, and distribution. The intent of the Pathfinder Programme is not only to provide easier access to archived data, but also to prepare the research community and the Data Archive Distribution Centers (DAACs) so that the onslaught of data expected from spaceborne sensors in the near future will be used effectively. The Pathfinder data

sets that are now available (Maiden and Greco 1994) to the research community can be used for addressing a wide range of climate-related issues.

The Pathfinder development effort encompasses data from several sensors. The AVHRR Land Pathfinder team (Townshend 1994) has nearly completed processing of more than 12 years of AVHRR GAC data from the NOAA-7, NOAA-9, and NOAA-11 satellites, at a spatial resolution of 8 km. The LANDSAT Pathfinder effort, in collaboration with NASA, USGS, and EPA, will build a three-year global data set (Schwaller *et al.* 1993) at a spatial resolution of 80 m. The NASA/NOAA SSM/I and SSMR Pathfinder data sets will produce long-term low-resolution data sets (at 12.5, 25, and 50 km spatial resolution) of several geophysical products. A global 1 km Pathfinder data set (Eidenshink and Faundeen 1994), constructed from AVHRR Local Area Coverage (LAC) data, is currently in production. In other words, the final goal of the Pathfinder Programme is to provide the research community with a long-term, high-quality data set from existing satellites.

The role of aerosols on the radiation balance of the Earth-atmosphere system has been well established (Penner *et al.* 1992, Charlson *et al.* 1990, 1992). Each year, increasing amounts of aerosols are released into the atmosphere due to biomass burning, dust storms, forest fires, and volcanic activity. These aerosol particles modify the radiative balance by reflecting the solar radiation back to space, called the 'direct effect' (Penner *et al.* 1992), and enhance the reflectivity of clouds by acting as cloud condensation nuclei (Charlson *et al.* 1992, Kaufman and Nakajima 1993), which is called the 'indirect effect'. For example, Penner *et al.* (1992) estimate that nearly 114Tg of smoke is produced in the tropics due to biomass burning, which could partially offset the warming expected from a doubling of CO<sub>2</sub>. These aerosol particles significantly affect the radiative balance on both regional and large scales.

Most biomass burning occurs in tropical countries (Hao *et al.* 1990, Crutzen and Andreae 1990) due to savanna fires, shifting cultivation practices, deforestation, fuel wood use, and burning of agricultural residues (Hao and Liu 1994). Although biomass burning activities are intense in the dry season, which is between December and March in the Northern Hemisphere, and between June and September in the Southern Hemisphere, burning can take place whenever there is plant material dry enough to burn (Andreae 1991). In South America, forest fires dominate the *selva* (forest) region (5°S–10°N; 60°–80°W; and between 5°–20°S and 40°–65°W), while agricultural burning due to savanna fires is widely prevalent in the *cerrado* region (5°–20°S and 40°–70°W). Fuel wood is burned mostly between 0°–30°S in Brazil. The major source of agricultural residue burning in South America is due to sugar cane and is concentrated around 5°S, 50°W; 20°S, 55°W, and 25°S, 55°W. Due to these activities, there is widespread concern about the loss of biodiversity (Uhl *et al.* 1988), the spread of human and plant diseases via colonization, the increase in concentrations of greenhouse gases (Greenberg *et al.* 1984), the effects on atmospheric chemistry (Fishman *et al.* 1986), a decrease in evapotranspiration (Shukla *et al.* 1990), and an increase in surface albedo and water runoff (Gentry and Lopez-Parodi 1980). The implications of these activities on regional and global scales are relatively unknown. The reduced resolution data sets that are now available as part of the AVHRR Land Pathfinder programme provide an opportunity to examine several important issues, including the spatial distribution of fires (Belward *et al.* 1994), ecosystem dynamics and cropping practices (Malingreau 1986), and vegetation mapping (Justice *et al.* 1985). Although high spatial resolution imagery from LANDSAT and AVHRR Local Area Coverage (LAC) provide more detailed information, these

data are difficult to obtain, expensive, and are not available over long enough time periods.

There is widespread concern that human activities are altering the climate and the nature of ecosystems (Charney 1975, Dickinson 1983). The tropical rainforest has received much attention (Henderson-Sellers and Gornitz 1984, Gash and Shuttleworth 1991, Potter *et al.* 1975) due to the high rates of deforestation (Salati and Vose 1983, Skole and Tucker 1993) from forest fires and fires due to various agricultural practices (Hao and Liu 1994). In tropical rainforests, albedo, along with surface roughness, appears to be the important factor which affects land surface and climate (Gash and Shuttleworth 1991). The change in vegetation and associated change in albedo could lead to changes in evapotranspiration and rainfall from altered general circulation patterns (Nobre *et al.* 1991). There is also modelling evidence that suggests tropical rainforests tend to be replaced by degraded grass (pasture) due to the reduced albedo and evapotranspiration (Nobre *et al.* 1991). Therefore, it is critical that the relation between the vegetation and the albedo be investigated over a sufficiently long period of time so that the role of fires in modifying the nature of the ecosystems is clearly defined. In this regard, more than 12 years of the AGLP data can provide the necessary data base.

The major focus of the present study is to examine the potential of the AVHRR GAC Land Pathfinder (AGLP) data set for aerosol and earth radiation budget studies. One month of AGLP data over South America from September 1985 is used, first to obtain the spatial and temporal distribution of fires; second, to collocate measurements from the ERBE scanner to examine the top of atmosphere radiative impact of smoke aerosols; and third, to examine the relation between NDVI and clear sky albedo during those days when smoke and clouds are not present. Specifically, this study demonstrates the potential of collocated AGLP and ERBE data to examine the effect of fires on the surface characteristics (NDVI and albedo) and the top of atmosphere regional radiative energy budget. A recent study by Belward *et al.* (1995) has already shown the usefulness and the potential of the AGLP data for mapping fires in West Africa. The present study is focused upon the South American region.

## **2. Data**

### **2.1. The AGLP data**

The creation of the AGLP data set is fully explained in James and Kalluri (1994). A brief description is given here for sake of completeness. The AVHRR GAC level 1B data set is used as input to the AGLP data processing scheme. Navigation of the image data is performed by using an orbital model and updated ephemeris (Rosborough *et al.* 1994). The radiances from channels 1 and 2 are converted to reflectances, and the radiances from channels 3, 4, and 5 are converted to brightness temperatures (Kidwell 1991). Corrections for the degradation of channels 1 and 2 are computed from Rao (1993), and corrections for the non-linear calibration of channels 4 and 5 are taken from Rao *et al.* (1993). Atmospheric corrections for Rayleigh scattering and ozone are performed following Gordon *et al.* (1988). However, no corrections are made for water vapour. A Goodes Interrupted Homolosine Projection at a resolution of 8 km (Steinwand 1994) is used for mapping. This mapping technique allows the best equal area representation of the data and allows for rapid subsetting and display capabilities. The values from the AVHRR channels 1 through 5 are output for each 8 km grid based on a forward binning

procedure. This method finds the location of a satellite pixel which is then used to locate the output bin. Note that there is no interpolation or averaging of the original AVHRR GAC pixel. However, at nadir, up to six GAC pixels can be mapped to a single 8 km output bin. The NASA Pathfinder scheme presently selects the 'greenest' pixel based on the Normalized Difference Vegetation Index (NDVI) to fill that bin, and this sampling biases the results towards less cloudy conditions (Belward *et al.* 1995). Along with the five channels of data, quality control flags and pertinent sun-satellite angles also are provided. In addition, an ancillary data set that includes latitude, longitude, elevation, and land/sea mask is available. The AGLP data set also provides a cloud mask index based on the CLouds from AVHRR (CLAVR) algorithm (Stowe *et al.* 1991). In the CLAVR algorithm, eleven tests are performed to classify a pixel as being either cloudy, cloud-free, or mixed. The AGLP data set produces both daily and ten-day composites from the afternoon satellites (NOAA-7, NOAA-9 and NOAA-11) from July 1981 to the present. The daily data set is used in this investigation and is restricted for viewing angles between  $\pm 30^\circ$  to avoid bi-directional effects.

### 2.2. *The Earth Radiation Budget Experiment scanner data*

The ERBE instrument (Barkstrom *et al.* 1989), which was launched in 1984 by NASA, has given the research community unique insights into the radiation balance of the earth-atmosphere system (for example, Hartmann *et al.* 1986, Ramanathan and Collins 1991). In addition, ERBE scanners were mounted on the NOAA-9, NOAA-10, and the ERBS platforms. The ERBE scanners, with a nominal spatial resolution of about 40 km (Kopia 1986), measured broadband radiances ( $0.25\ \mu\text{m}$ – $4\ \mu\text{m}$  and  $4\ \mu\text{m}$ – $50\ \mu\text{m}$ ), which were then converted to TOA fluxes by using Angular Dependence Models (ADM's) (Suttles *et al.* 1988, 1989). Since the scanner on NOAA-9 was operational between February 1985 and January 1987, the radiative impact of two biomass burning seasons can be analysed. In particular, by collocating measurements from the narrowband AVHRR data and the broadband ERBE data, the radiative impact of aerosols on the earth-atmosphere system can be investigated.

### 2.3. *Area of study*

In the present investigation, the daily AGLP data from September 1985 are used. The area of study is roughly between  $0^\circ$  to  $-20^\circ\text{S}$  and  $43^\circ\text{W}$  to  $72^\circ\text{W}$  and is shown in figure 1. There are four major ecosystems within this region, based upon the Olson world ecosystem database (Olson 1992). The four ecosystems are: tropical rain forest (TRF); tropical broadleaf seasonal (TBS), with dry or cool season; savanna/grass, and seasonal woods (SGW)†; and mild/warm/hot/grass/shrub (MGS). In other studies, Prins and Menzel (1994), this study region is broadly classified as either *selva* (rainforest), mixed (broadleaf and savanna), or *cerrado* (grassland). This area of study has been the subject of many other investigations (for example, Malingreau *et al.* 1989, Malingreau and Tucker 1988, Ward *et al.* 1992) due to the high rates of deforestation and other agricultural practices. Although much effort has gone into obtaining the spatial and temporal distribution of fires, there exists no comprehensive information on the regional radiative impact of aerosols produced from burning.

---

†In this category, trees or shrubs above grass ground cover may be interspersed in many scales in savanna belts of varying drought duration and high fire frequency.

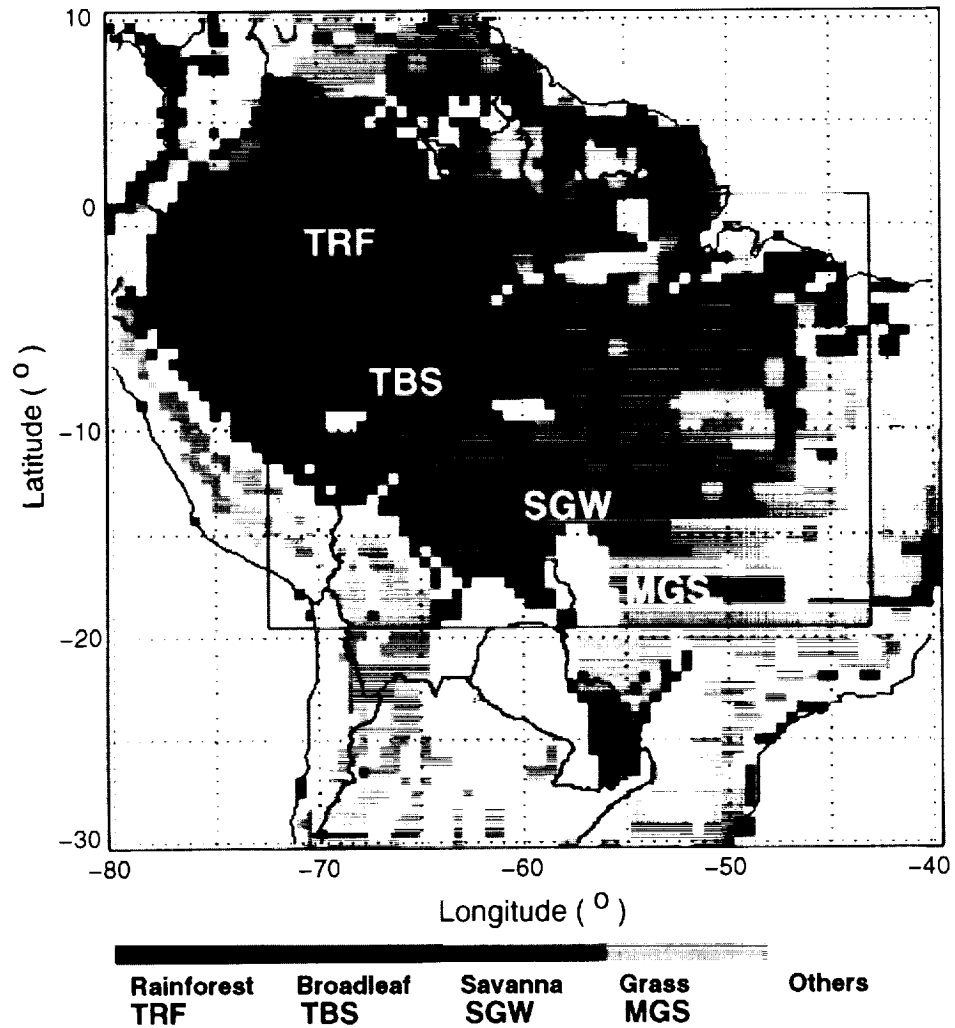


Figure 1. Ecosystem characterization from Olson (1992) with area of study shown by the rectangle.

### 3. Methodology

The AGLP data are currently being received from the NASA's Goddard Space Flight Center (GSFC) on 4 mm DAT tapes (Agbu and James 1994). The data volume for each day is rather large, on the order of 250 Mb. Each file contains: (1) the Normalized Difference Vegetation Index (NDVI); (2) the CLAVR cloud masking flags; (3) quality control flags; (4) relevant Sun-satellite geometry angles; (5) AVHRR channel 1-5 values; and (6) the day of the year. These data are made available for Africa, Asia, Australia, Europe, North America, and South America. Note that the data are only provided over land. Subsetting tools are also provided to analyse either the individual channels or selected continents. The data is in hierarchical data format (HDF) format; even with subsetting tools, the data volume is rather difficult to handle. Although the HDF format is quickly becoming the standard for remotely-sensed data, efficient ways for storing and distributing the data must be explored.

### 3.1. Fire detection

Fires are detected following the method of Kaufman *et al.* (1990). In this method, a pixel is labelled as containing fire if it satisfies the following conditions:

$$\begin{aligned} T_3 &\geq 316 \text{ K} \\ T_3 &\geq T_4 + 10 \text{ K} \\ T_4 &> 250 \text{ K} \end{aligned} \quad (1)$$

where  $T_3$  and  $T_4$  are AVHRR channel 3 and channel 4 temperatures. The first condition ensures that the channel 3 temperatures are closer to the saturation level. The second condition ensures that the hot shrub and grass are not included as fire pixels. The third condition ensures that the pixel is not contaminated with strongly reflective clouds. Due to the different background conditions, Belward *et al.* (1995) and Franca *et al.* (1995) use different conditions for detecting fires over West Africa. However, a GAC pixel can be classified as a fire pixel only if the original AVHRR Local Area Category (LAC) pixels all had fire. Therefore, in the present study, the number of fires are adjusted for the GAC resolution (Belward *et al.* 1994) when actual fire counts are performed. Although spatial averaging of the AVHRR LAC data reduces the fire counts (Belward *et al.* 1994), it is useful to determine the spatial extent of the fires from the AGLP data set.

### 3.2. Detection of smoke

The smoke aerosols produced from biomass burning can be broadly classified into two categories. The first is the dense smoke category, or areas with heavy aerosol loading, which is found over the active and smoldering fires and is comprised of smoke aerosols. The second category is the haze-like smoke which has been transported by the meteorological conditions to several hundreds of kilometres. These haze-like conditions are found throughout the biomass burning season in South America (Andreae *et al.* 1988) and could have a significant impact on the regional radiative balance.

In the present study, a combination of spectral and textural measures is used to separate visually the aerosols from the underlying background (Christopher *et al.* 1996). The normalized AVHRR channel ratio of  $(1-4)/(1+4)$  is first used to produce an image. This image then is used to compute several textural measures (Welch *et al.* 1988a, b, Tovinkere *et al.* 1993) for a  $9 \times 9$  pixel window. The textural measure that best produces a visual separation between the aerosols and the underlying background is then used to create a three-band overlay image. The textural measure that produces the best results was the 'mean' value. Although the channel ratio of  $(1-4)/(1+4)$  is sensitive to both smoke and clouds, it is the combination of spectral (channel 1,  $(1-4)/(1+4)$ ) and textural measure (mean) that provides a good visual separation between the surface and aerosol features.

Figure 2 shows a three-band overlay of one image from 3 September 1985 over South America. The AVHRR channel 1 is in red, the normalized AVHRR channel combination of  $(1-4)/(1+4)$  is in green, and the 'mean' textural measure of channel  $(1-4)/(1+4)$  is in blue. Each channel is histogram equalized. The fires are coloured in red (which were detected using the technique described in section 3.1), and the image has been enlarged by a factor of 2 for clarity of presentation. Several interesting features can be seen in this image. The background appears dark due to the dense vegetation, the clouds appear white, and the haze appears to be light yellow. The



Figure 2. Three-band overlay of the AGLP data on 3 September 1985 in which channel 1 is in red, normalized channel ratio of  $(1 - 4)/(1 + 4)$  in green, and the mean textural measure of  $(1 - 4)/(1 + 4)$  in blue.

dense smoke plume labeled 'P' toward the middle of the image in Rondonia is bright yellow in colour, and there are a number of fires in the Matto Grosso area. More than 1500 pixels were classified as 'fire' from this image. The dense smoke plume was also verified using the AVHRR LAC imagery (Christopher *et al.* 1996). Also shown, in blue, are several sample ERBE scanner footprints (see section 3.4) over the area of interest. Note the jagged appearance toward the edge of the swath; this is due to the overlap of the AVHRR swaths and the forward binning procedure that is inherent in the AGLP data processing scheme. Figure 2 is a typical example of AGLP imagery over South America and is merely shown to demonstrate the spatial extent of fire and smoke in the Amazon Basin.

Figure 3 shows the channel 3 and channel 4 temperatures from the AGLP data set for the transect A-B shown in figure 2. The dense smoke plume, labelled P in figure 2, around pixel number 250 shows a difference of about 12 K to 15 K between channel 3 and channel 4 temperatures. This difference in temperatures between channel 3 and channel 4 makes the detection of fires possible from satellite imagery. Even at a coarse spatial resolution, the AGLP data set shows the sensitivity of channel 3 temperatures to the fires.

#### 3.4. Collocation of AVHRR with ERBE data

Since the AVHRR and the ERBE scanner were both mounted on board the NOAA-9 satellite, coincident measurements are available for the two years that the

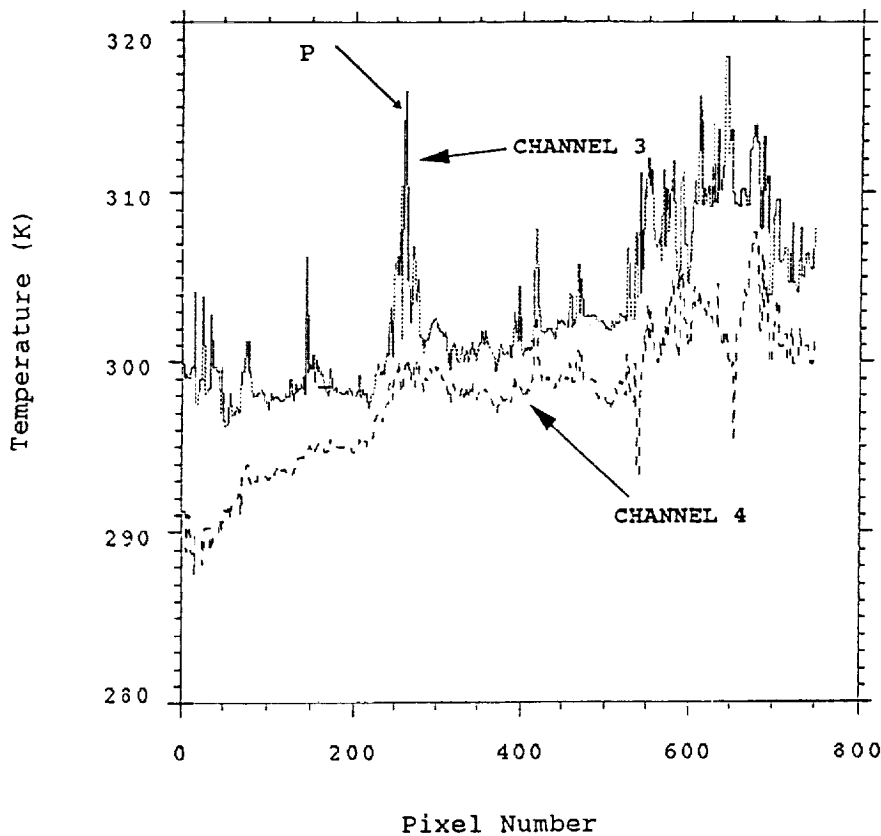


Figure 3. AGLP channel 3 and channel 4 temperatures for transect (A-B) shown in figure 2.



scanner was operational. The ERBE-measured radiances are converted to top-of-atmosphere fluxes (Barkstrom *et al.* 1989) using a maximum likelihood estimation (MLE) technique (Wielicki and Green 1989) and angular dependence models (Suttles *et al.* 1988, 1989). The ERBE scene identification classifies a pixel as either clear, partly cloudy, mostly cloudy or overcast. The geographical regions with aerosols tend to be misclassified as being partly cloudy or mostly cloudy (Ackerman and Chung 1992), thereby resulting in errors in top-of-atmosphere (TOA) fluxes. A technique described in the next paragraph provides for more reliable scene identification. The maximum errors by assuming the inappropriate bidirectional and limb-darkening models for shortwave flux are about 14 per cent, and are negligible in the longwave (Diekmann and Smith 1989). Until realistic limb darkening and bi-directional models are developed for aerosols, the ERBE measurements provide the only method for estimating the direct radiative impact of aerosols using satellite data.

Since the ERBE scanner has a footprint which is about five times larger than the Pathfinder output bin, a group ( $5 \times 5$ ) of AVHRR pixels that corresponds to the AGLP data is first identified. Then the average channel 1 reflectances and channel 4 temperatures for that group of pixels are correlated with the ERBE shortwave and longwave fluxes, respectively. Figures 4(a) and 4(b) show the correlation between the AGLP channel 1 reflectance and the ERBE shortwave flux (linear correlation coefficient: 93 per cent) from 3 September 1985, and between the AGLP channel 4 temperatures and the ERBE longwave fluxes (linear correlation coefficient: 95 per cent), respectively. Correlation coefficients greater than 90 per cent ensure that the AGLP and the ERBE data have been properly calibrated, navigated, and collocated. This provides an indirect method for validating the two data sets. After a group of AVHRR pixels has been identified, the CLAVR flags are used to further divide the  $5 \times 5$  AGLP pixels into four categories, as shown in table 1.

By using the CLAVR flags, this scene identification scheme is more reliable than the ERBE scene identification scheme, since narrowband radiometers such as AVHRR provide more spectral and spatial information as opposed to the ERBE broadband measurements. This technique of combining narrowband and broadband measurements is a powerful tool in climate studies (see Ackerman and Inoue 1994, Ackerman *et al.* 1992, Li and Leighton 1991).

#### 4. Results

The results are divided into the following sections. First, the spatial and temporal distribution of the fires is examined as a function of four ecosystems for September 1985. Then, the TOA SW and LW fluxes for dense smoke are computed. The final section discusses the relationship between the ERBE clear sky albedos and the AGLP derived NDVI.

##### 4.1. Spatial and temporal distribution of fires

In this section, the spatial and temporal distribution of fires as a function of four ecosystems is discussed. Figures 5 (a-d) show the number of fire pixels for each day in September 1985 for TRF, TBS, SGW, and MGS. The number of fires has been adjusted to account for the AGLP spatial resolution following Belward *et al.* (1994). The number of fires in TRF is much less compared to the other three ecosystems. Maximum fire events are in the grassland. The peak fire activities for SGW are

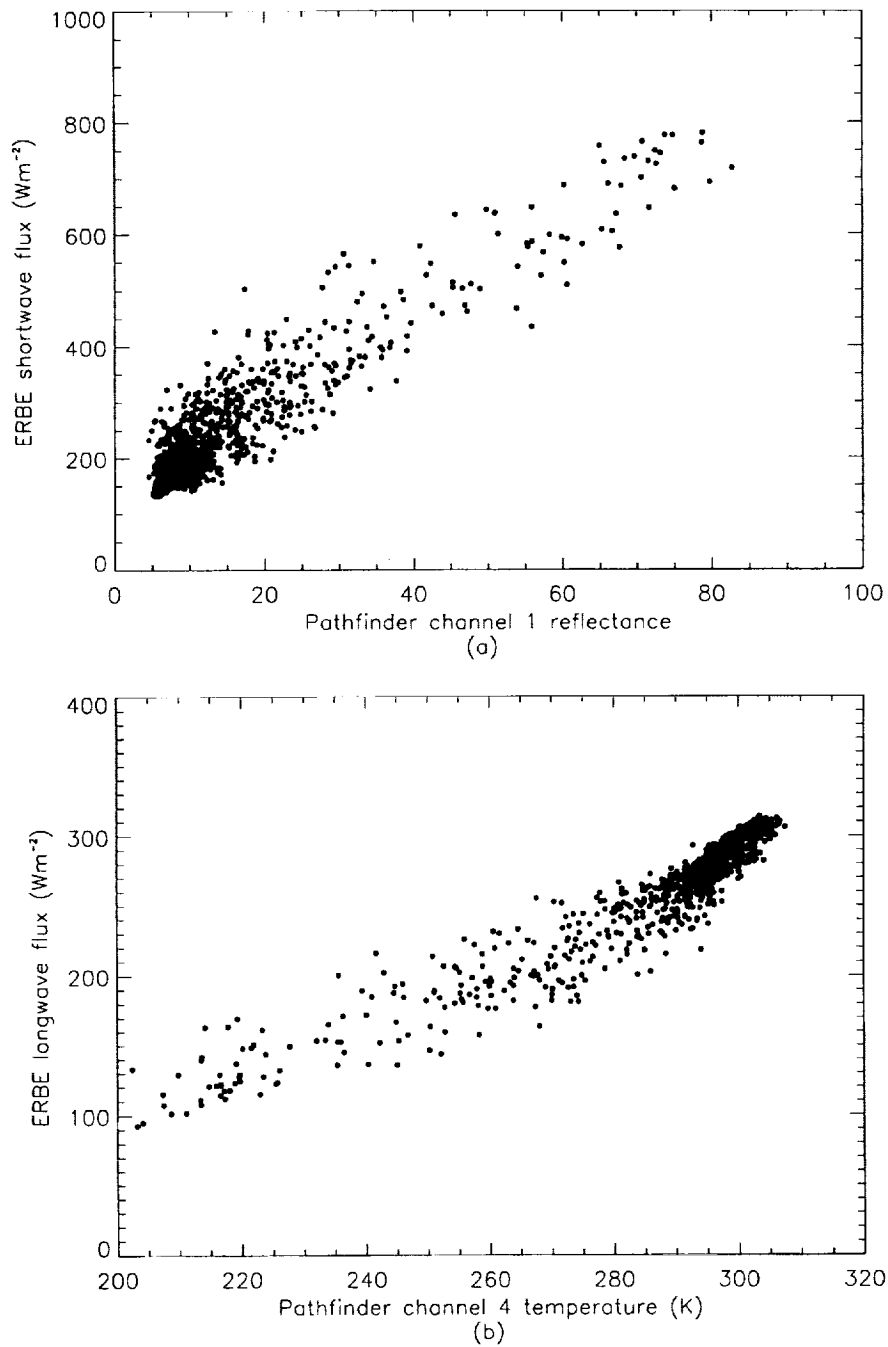


Figure 4. Scatter plot and correlation for (a) ERBE shortwave flux vs. AGLP channel 1 temperature; and (b) ERBE Longwave flux vs. AGLP channel 4 temperature.

during the beginning of the month, and for the TBS and MGS ecosystems during mid- to late-September. There is a well-defined temporal change in the number of fires for the TBS, SGW, and the MGS ecosystems.

Table 1. Classification of ERBE pixels based on AGLP data.

Percentage of AGLP pixels classified as cloudy	ERBE pixel labelled as
0–5	Clear
5–50	Partly cloudy
50–95	Mostly cloudy
95–100	Overcast

#### 4.2. The ERBE top of atmosphere (TOA) fluxes for dense smoke

In order to examine the TOA radiative impact produced from biomass burning, each AGLP image is used to separate the dense smoke from cloudy conditions by using a simple infrared threshold. If within a collocated ERBE pixel, a fire or a group of fires was detected, the SW and LW fluxes were assumed to be from smoke, provided the channel 4 temperatures were greater than 250 K. This method does have the drawback of sometimes identifying low clouds warmer than 250 K as smoke. However, a visual examination of several AVHRR LAC images from the 1985 and 1987 biomass burning seasons over South America (Christopher *et al.* 1996), shows that directly above fires, in most cases smoke is present, as opposed to low clouds. For the labelling of clear sky pixels, the CLAVR flag was used. If 95 per cent of the AGLP pixels within the ERBE footprint were identified by the CLAVR algorithm as being clear, then that ERBE pixel was classified as being clear sky. The majority of the pixels identified as clear from the ERBE scheme were classified as partly cloudy or mostly cloudy by the CLAVR method. This shows the difficulty in using broadband measurements for identifying clouds, aerosols and surface features and the importance of augmenting them with narrow band AVHRR data. More than 70 per cent of the smoke pixels were classified by both ERBE and AVHRR as being partly cloudy or mostly cloudy.

Figures 6(a–d) show the frequency histograms of shortwave flux for four ecosystems and figures 6(e–h) show the corresponding longwave fluxes. The solid lines denote the clear sky histograms and the pixels identified as smoke are shown in dotted lines. The number of collocated pixels identified as clear sky and smoke are annotated for the four ecosystems in figures 6(a–d). For example, there are 198 collocated ERBE pixels identified as being clear in the MGS ecosystem and 1553 as dense smoke aerosols. The TRF ecosystem has the fewest pixels identified as smoke, since there were not many fires, as discussed in section 4.1. The other ecosystems have adequate samples for clear sky and smoke representation. The peak clear-sky shortwave flux values are between 160–200 W m<sup>-2</sup> for the four ecosystems, while the areas with heavy aerosol loading have peak SW flux values between 200–240 W m<sup>-2</sup> for TBS, SGW, and the MGS ecosystems, and between 240–280 W m<sup>-2</sup> for the TRF ecosystem. For all four ecosystems, the SW flux values are higher for smoke than that over clear land, which shows the importance of smoke aerosols in modifying the shortwave energy budget of the Earth–atmosphere system.

While there appears to be a significant impact between the smoke aerosols and the underlying background in the shortwave part of the spectrum (0.25–4 μm), it is rather difficult to discern the effect of aerosols in the longwave (4 to > 50 μm) part of the spectrum. The TRF ecosystem shows that the longwave flux from the smoke aerosols are lower than that of clear land. However, the results from the TRF

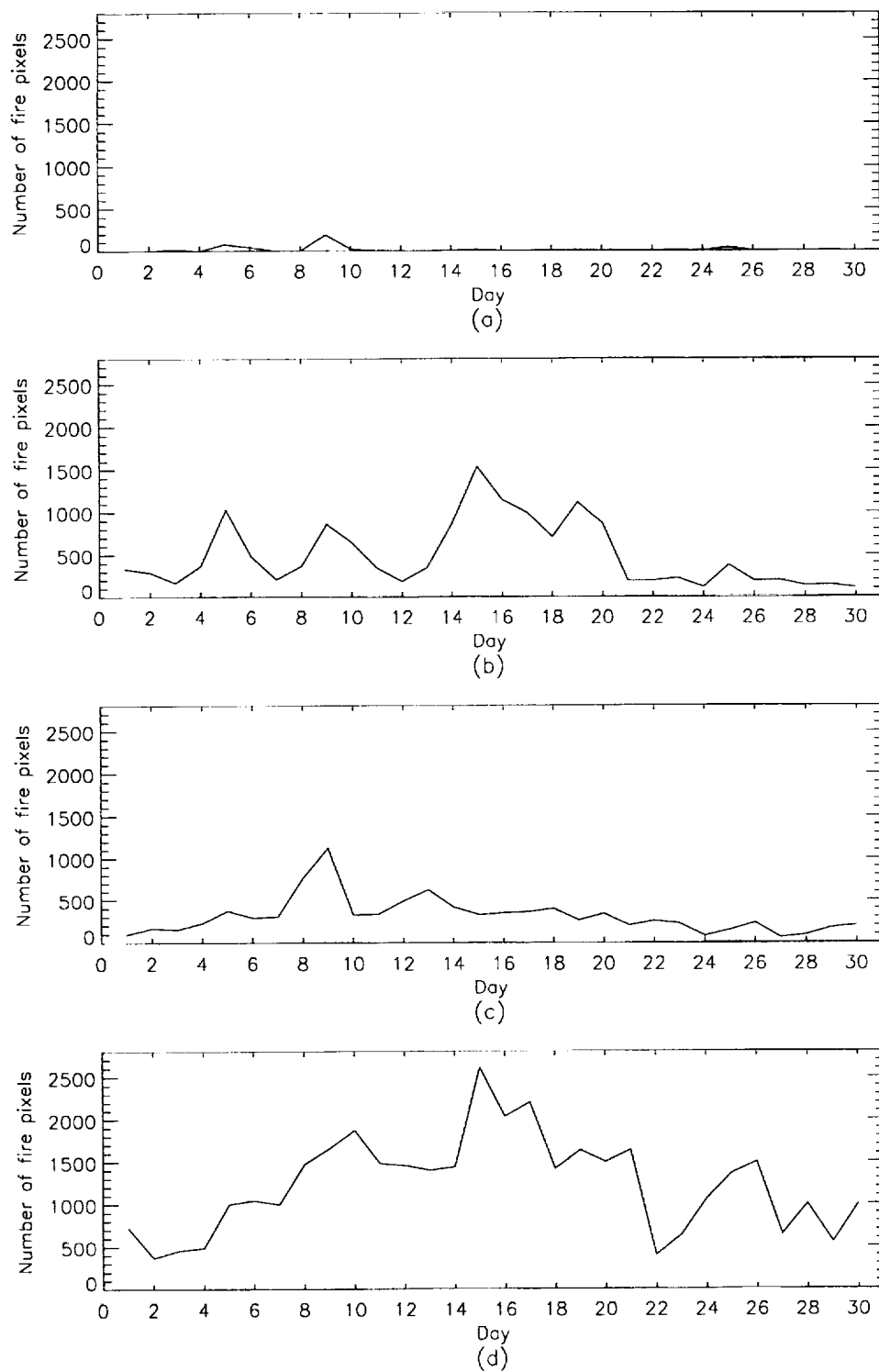


Figure 5. Temporal distribution of fires for four ecosystems: (a) tropical rainforest; (b) broadleaf; (c) savanna; and (d) grassland.

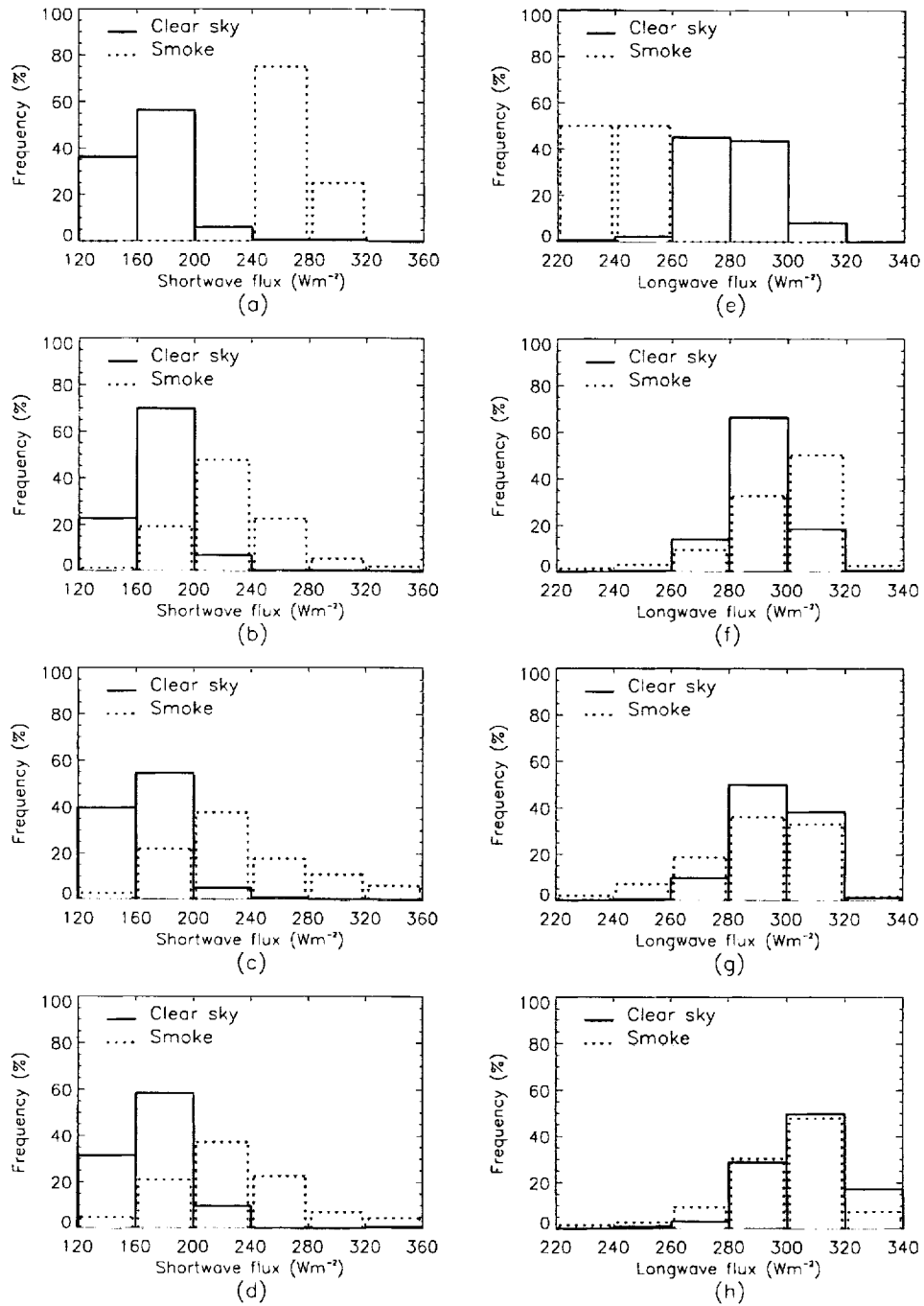


Figure 6. Frequency distribution of dense smoke and clear-sky pixels from collocated measurements (a-d) shortwave flux; and (e-h) long-wave flux, for four ecosystems. The solid line is for clear sky and the dotted line is for dense smoke. The number of collocated clear sky pixels for the four ecosystems are 98, 707, 850 and 198 respectively. The number of smoke pixels are 8, 643, 584, 1553.

category should be interpreted with caution because there are only eight collocated samples. The clear sky longwave flux values, which could be converted to temperatures, show a large variation even within each ecosystem category. For example, the MGS ecosystem has peak LW flux values between  $300\text{--}320\text{ W m}^{-2}$  with a few collocated pixels having clear-sky LW flux values of as low as  $240\text{ W m}^{-2}$  and as high as  $340\text{ W m}^{-2}$ . This spread in LW flux values of about  $100\text{ W m}^{-2}$  shows the varying temperatures across the grassland areas of the Amazon Basin. Finally, it is noted that the longwave flux values are similar for both the clear-sky and the smoke aerosols. This is probably due to the fact that the ERBE footprints are only partially-covered by smoke aerosols. This produces higher LW flux values due to the fact that the signal emanates from the aerosol layer and the background. On the other hand, even though the smoke aerosols partially cover the ERBE footprint, the highly-reflective nature of these aerosols tends to increase the SW signal above the background values.

#### 4.3. Relation between NDVI and ERBE broadband albedo

In this study, collocated clear sky pixels, as determined by the CLAVR algorithm, are used to obtain the Normalized Difference Vegetation Index (NDVI), provided as part of the AGLP data set. The TOA clear sky fluxes from ERBE are used to obtain instantaneous clear sky albedos. Both the clear sky albedos and NDVI statistics were accumulated during those days when smoke and clouds were not present. The NDVI has been correlated with green-leaf biomass and green-leaf area, and is widely used to discriminate vegetation (for example, Curran and Williamson 1987, Holben *et al.* 1980). Figures 7(a–d) show the frequency histograms of NDVI for clear sky pixels for the four major ecosystems under consideration: (a) TRF; (b) TBS; (c) SGW, and (d) MGS. Figures 7(e–h) show the corresponding clear sky albedos determined from the ERBE scanner data. In figures 7(a–d), a well-defined NDVI relationship is found between the four ecosystems, with the peak NDVI values for TRF between 0.5–0.6; for TBS between 0.3–0.4; for SGW between 0.2–0.3 and for MGS between 0–0.1. This relationship between NDVI and ecosystem could be due either to less vegetation or drying vegetation. Note that although peak values are different for these four ecosystems, the spread in NDVI values are quite large (0.2 to 0.6 for TRF; –0.1 to 0.6 for TBS; –0.1 to 0.6 for SGW and –0.2 to 0.6 for MGS) and indicate the variability within each ecosystem. The small percentage of pixels with negative NDVI values are probably due to uncertainties in the navigation or due to water contamination.

Clear sky albedos are between 14 to 25 per cent for all four ecosystems. The TRF shows a slightly lower peak clear sky albedo when compared to the other three ecosystems. In order to understand the correlation between NDVI and clear sky albedo, figures 8(a–d) shows a scatter plot between the two parameters for the four ecosystems. In all four cases, the correlation coefficients are negative, which shows that as clear sky albedos increase, the corresponding NDVI values decrease. The TRF has the smallest range of NDVI's and clear sky albedos with the highest correlation coefficient. Some of the variability could be attributed to the atmospheric variability and instrument characteristics. Also note that in figure 8(d), the slope for the relationship between NDVI and albedo is different from that in figures 8(a–c). Using this kind of analysis, seasonal and yearly trends in the radiation budget can now be examined as a function of burned areas, land use change, and so on, on tropical ecosystems.

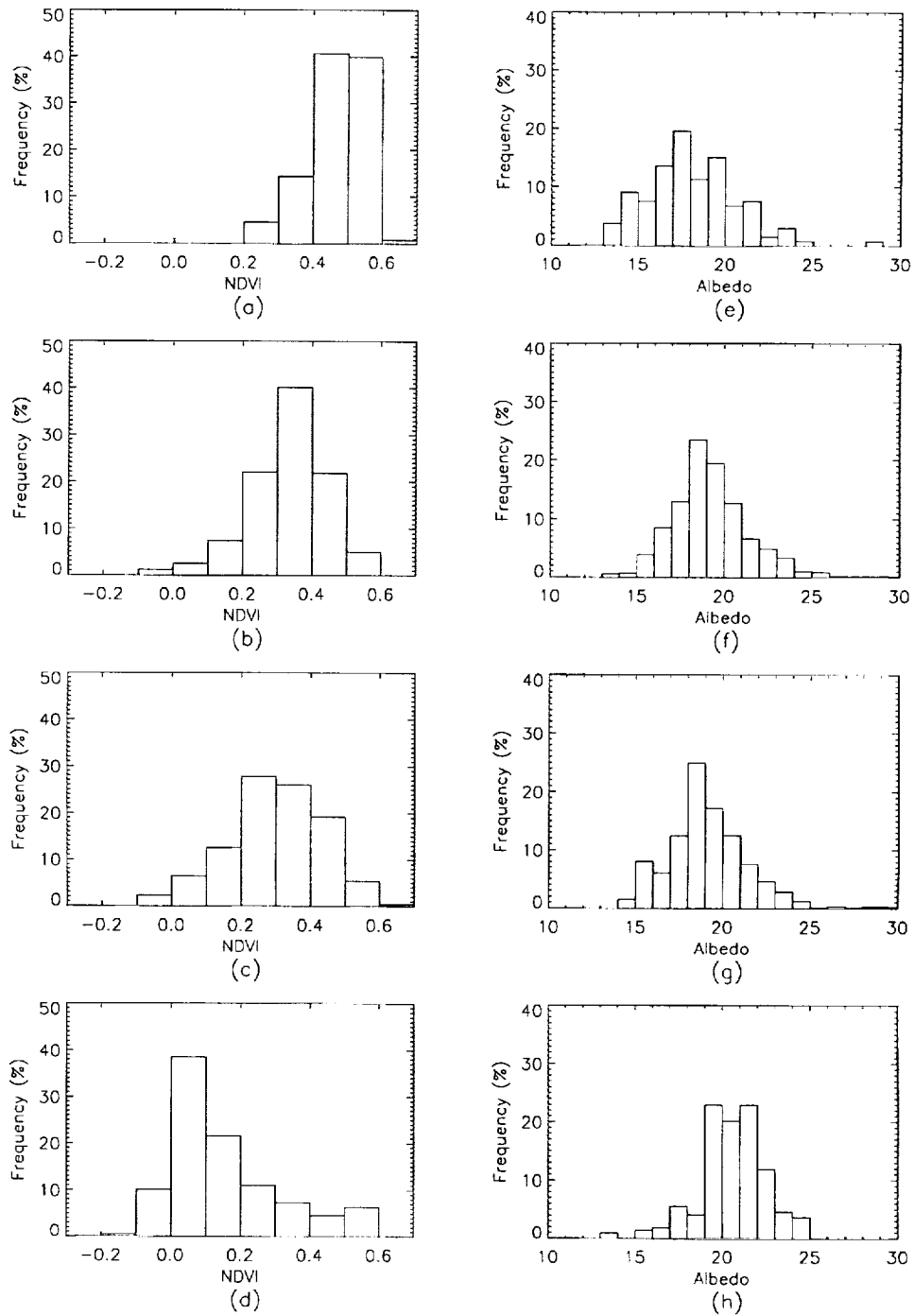


Figure 7. Frequency distribution of NDVI (a-d) and ERBE clear sky albedo (e-h) for four ecosystems.

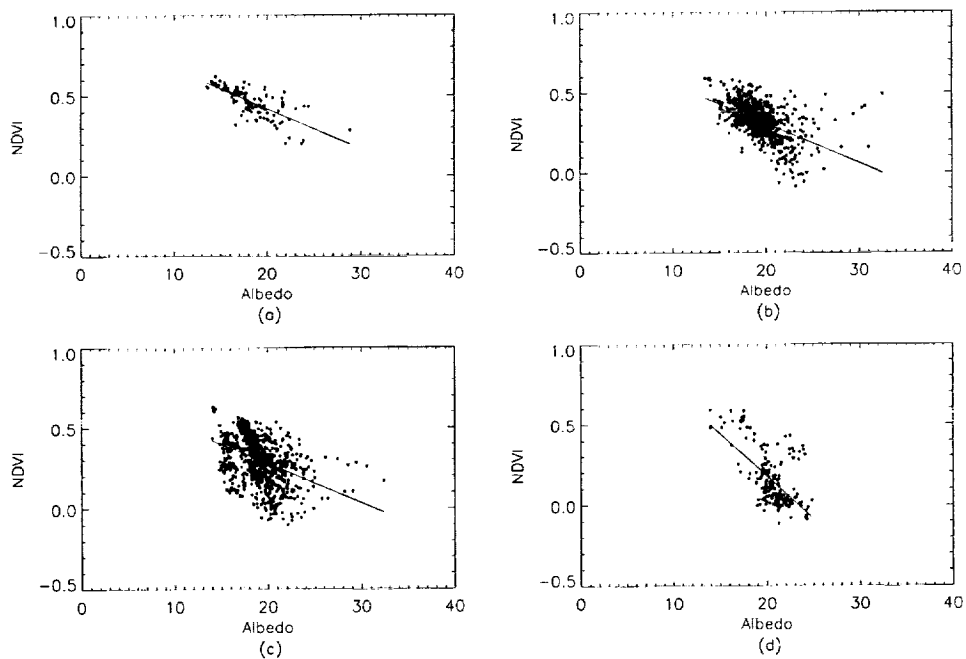


Figure 8. Relation between ERBE clear sky albedo and AGLP-derived NDVI for four ecosystems: (a) tropical rainforest; (b) broadleaf; (c) savanna; and (d) grassland.

### Conclusions

In this study, the potential of the NASA AGLP data and coincident ERBE data are explored for addressing the role of fires on four major ecosystems in South America. One month of data from September 1985 is used to examine the spatial and temporal distribution of fires. Collocated measurements from the ERBE scanner are also used to examine the regional TOA radiative impact of smoke pixels directly over the fires. When smoke and clouds are not present, ERBE clear sky albedos are correlated with the NDVI values.

The four major ecosystems in the area of study show a well-defined temporal variation of fires. The grassland ecosystem has the highest number of fires and peak values are found during mid- to late September in 1985. On the other hand, the number of fires over the tropical rainforest are significantly less. It is emphasized again, that although it is difficult to obtain the absolute number of fires from reduced resolution imagery (Belward *et al.* 1994), it is nevertheless useful to obtain the spatial distribution of fires.

The TOA shortwave fluxes for smoke pixels directly over the fires are higher than that of clear land, which shows the importance of smoke in modifying the regional radiative balance, while the longwave fluxes for both the clear and aerosol regions are similar.

The NDVI values derived from the AGLP data show that the peak values for the tropical rainforest are higher than that of broadleaf, savanna, and grassland, although there is a well-defined spread in NDVI values for each ecosystem. The clear sky albedos show a negative correlation with the NDVI values. For all four ecosystems, as NDVI values decreased, the corresponding broadband ERBE clear sky albedos increased.



This study, although from one month of analysis, shows that the AGLP data set has good potential for studying several climate-related issues such as spatial extent of fires and vegetation mapping. The appropriate use of collocated data from other instruments such as the ERBE scanner will provide information on the role of vegetation or land use change in modifying the albedo. These results could also be used to verify land surface feedback processes in general circulation models (GCMs). A long-term analysis of the AGLP data could reveal vital information on the role of anthropogenic activities on land. Although the Pathfinder team has successfully completed one of its objectives by providing the research community with a long-term data set, there needs to be adequate resources to analyse these data and realize the final objectives of the Pathfinder and the Global Climate Change programme.

#### Acknowledgments

This research was funded by NASA Grants NAGW-3966 and NAGW-3740, both managed by Dr Robert J. Curran. The Pathfinder data used by the authors in this study include data produced through funding from the Earth Observing System Pathfinder Program of NASA's Mission to Planet Earth in cooperation with National Oceanic and Atmospheric Administration. The data were provided by the Earth Observing System Data and Information System, Distributed Active Archive Center at Goddard Space Flight Center, which archives, manages and distributes the data set. The ERBE S-8 data were obtained from the NASA Langley Research Center EOSDIS Distributed Active Archive Center. Special thanks to Rand E. Feind and Ronald M. Welch for their useful comments. Appreciation is extended to Connie Crandall for organizing this manuscript.

#### References

- ACKERMAN, S. A., and CHUNG, H., 1992, Radiative effects of airborne dust on regional energy budgets at the top of the atmosphere. *Journal of Applied Meteorology*, **31**, 223–233.
- ACKERMAN, S. A., FREY, R. A., and SMITH, W. L., 1992, Radiation budget studies using collocated observations from AVHRR, HIRS/2 and ERBE instruments. *Journal of Geophysical Research*, **97**, 11513–11525.
- ACKERMAN, S. A., and INOUE, T., 1994, Radiation energy budget studies using collocated AVHRR and ERBE observations. *Journal of Applied Meteorology*, **33**, 370–377.
- AGBU, P. A., and JAMES, M. E., 1994, The NOAA/NASA Pathfinder AVHRR Land Data Set User's Manual. Goddard Distributed Active Archive Center, NASA, Goddard Space Flight Center, Greenbelt.
- ANDREAE, M. O., 1991, Biomass burning: Its history, use, and distribution and its impact on environmental quality and climate. In *Global Biomass Burning*, edited by J. S. Levine (Cambridge, MA: MIT Press), pp. 1–21.
- ANDREAE, M. O., BROWELL, E. V., GARSTANG, M., GREGORY, G. L., HARRIS, R. C., HILL, G. F., JAQCOB, D. J., PEREIRA, M. C., SACHSE, G. W., SETZER, A. W., SILVA DIAS, P. L., TABLOT, R. W., TORRES, A. L., and WOFSY, S. C., 1988, Biomass burning emissions associated with haze layers over Amazonia. *Journal of Geophysical Research*, **93**, 1509–1527.
- ASRAR, G., and DOKKEN, D. J., 1993, EOS Reference Handbook. NASA NP0202.
- BARKSTROM, B. R., HARRISON, E., SMITH, G., GREEN, R., KIBLER, J., CESS, R., and the ERBE Science Team, 1989, Earth Radiation Budget Experiment (ERBE) archival and April 1985 results. *Bulletin of the American Meteorological Society*, **70**, 1254–1262.
- BELWARD, A. S., KENNEDY, P. J., and GREGOIRE, J-M., 1994, The limitations and potential of AVHRR GAC for continental scale studies. *International Journal of Remote Sensing*, **15**, 2215–2234.
- BELWARD, A. S., HOLLIFIELD, A., and JAMES, M., 1995, The potential of the NASA GAC

- PATHFINDER product for the creation of global thematic data sets: the case of biomass burning patterns. *International Journal of Remote Sensing*, **16**, 2089–2097.
- CHARLSON, R. J., LANGNER, J., and RODHE, H., 1990, Sulphate aerosol and climate. *Nature*, **384**, 22.
- CHARLSON, R. J., SCHWARTZ, S. E., HALES, J. M., CESS, R. D., COAKLEY, JR., J. A., HANSEN, J. E., and HOFMANN, D. J., 1992, Climate forcing by anthropogenic aerosols. *Science*, **255**, 423–430.
- CHARNEY, J. G., 1975, Dynamics of deserts and drought and shale. *Quarterly Journal of the Royal Meteorological Society*, **101**, 193–202.
- CHRISTOPHER, S. A., KLICHE, D. V., CHOU, J., and WELCH, R. M., 1996, First estimates of the radiative forcing of aerosols generated from biomass burning using satellite data. *Journal of Geophysical Research—Atmospheres*, **101**, 21265–21273.
- CRUTZEN, P. J., and ANDREAE, M. O., 1990, Biomass burning in the tropics: impact on atmospheric chemistry and biogeochemical cycles. *Science*, **250**, 1669–1678.
- CURRAN, P. J., and WILLIAMSON, H. D., 1987, GLAI estimation using measurements of red, near-infrared, and middle-infrared radiance. *Photogrammetric Engineering and Remote Sensing*, **53**, 181–186.
- DICKINSON, R. E., 1983, Land surface processes and climate-surface albedos and energy balance. *Advanced Geophysics*, **25**, 305–353.
- DIEKMANN, F. J., and SMITH, G. L., 1989, Investigation of scene identification algorithms for radiation budget measurements. *Journal of Geophysical Research*, **94**, 3395–3412.
- EIDENSHINK, J. C., and FAUNDEEN, J. L., 1994, The 1 km AVHRR global land data set: first stages in implementation. *International Journal of Remote Sensing*, **15**, 3443–3462.
- FISHMAN, J., MINNIS, P., and REICHEL, JR., H. G., 1986, Use of satellite data to study tropospheric ozone in the tropics. *Journal of Geophysical Research*, **91**, 14451–14465.
- FRANCA, J. R., BRUSTET, J.-M., and FONTAN, J., 1995, Multispectral remote sensing of biomass burning in West Africa. *Journal of Atmospheric Chemistry*, **22**, 81–110.
- GASH, J. H. C., and SHUTTLEWORTH, W. J., 1991, Tropical deforestation: albedo and the surface energy balance. *Climate Change*, **19**, 123–134.
- GENTRY, A. H., and LOPES-PARODY, J., 1980, Deforestation and increased flooding in the upper-Amazon. *Science*, **210**, 1354–1356.
- GORDON, H. R., BROWN, J. W., and EVANS, R. H., 1988, Exact Rayleigh scattering calculations for use with NIMBUS-Coastal Zonal Color Scanner. *Applied Optics*, **7**, 2111–2122.
- GREENBERG, J. P., ZIMMERMAN, P. R., HEIDT, L., and POLLOCK, W., 1984, Hydrocarbon and carbon monoxide emissions from biomass burning in Brazil. *Journal of Geophysical Research*, **89**, 1350–1354.
- HAO, W. M., and LIU, M.-H., 1994, Spatial and temporal distribution of biomass burning. *Global Biogeochemical Cycles*, **8**, 495–503.
- HAO, W. M., LIU, M.-H., and CRUTZEN, P. J., 1990, Estimates of annual and regional releases of CO<sub>2</sub> and other trace gases to the atmosphere from fires in the tropics, based on the FAO statistics for the period 1975–1980. In *Fire in the Tropical Biota: Ecological Studies*, vol. 84, edited by J. G. Goldammer (New York: Springer-Verlag), pp. 440–462.
- HARTMANN, D. L., RAMANATHAN, V., BERROIR, A., and HUNT, G. E., 1986, Earth radiation budget data and climate research. *Reviews of Geophysics*, **24**, 439–468.
- HENDERSON-SELLERS, A., and GORNITZ, V., 1984, Possible climatic impacts of land cover transformations, with particular emphasis on tropical deforestation. *Climatic Change*, **6**, 231–257.
- HOLBEN, B. N., TUCKER, C. J., and FAN, C. J., 1980, Spectral assessment of soy-bean leaf area and leaf biomass. *Photogrammetric Engineering & Remote Sensing*, **45**, 651.
- JAMES, M. E., and KALLURI, S. N. V., 1994, The Pathfinder AVHRR land data set: an improved coarse resolution data set for terrestrial monitoring. *International Journal of Remote Sensing*, **15**, 3347–3364.
- JUSTICE, C. O., TOWNSEND, J. R. G., HOLBEN, B. N., and TUCKER, C. J., 1985, Analysis of the phenology of global vegetation using meteorological satellite data. *International Journal of Remote Sensing*, **6**, 1271–1318.
- KAUFMAN, Y. J., and NAKAJIMA, T., 1993, Effect of Amazon smoke on cloud microphysics and albedo-analysis from satellite imagery. *Journal of Applied Meteorology*, **32**, 729–744.

- KAUFMAN, Y. J., TUCKER, C. J., and FUNG, I., 1990, Remote sensing of biomass burning in the tropics. *Journal of Geophysical Research*, **95**, 9927–9939.
- KIDWELL, K. B., 1991, NOAA Polar Orbiter Data Users Guide. NOAA National Climatic Data Center, Satellite Data Services Division.
- KOPIA, L. P., 1986, Earth Radiation Budget Experiment scanner instrument. *Journal of Geophysical Research*, **89**, 400–406.
- LI, Z., and LEIGHTON, H. G., 1991, Scene identification and its effect on cloud radiative forcing in the Arctic. *Journal of Geophysical Research*, **96**, 9175–9188.
- MAIDEN, M. E., and GRECO, S., 1994, NASA's Pathfinder data set programme: land surface parameters. *International Journal of Remote Sensing*, **15**, 3333–3346.
- MALINGREAU, J. D., 1986, Global vegetation dynamics: satellite observations over Asia. *International Journal of Remote Sensing*, **7**, 1121–1146.
- MALINGREAU, J., and TUCKER, C. J., 1988, Large scale deforestation in the southeastern Amazon Basin of Brazil. *Ambio*, **17**, 49–55.
- MALINGREAU, J. P., TUCKER, C. J., and LAPORT, N., 1989, AVHRR for monitoring global tropical deforestation. *International Journal of Remote Sensing*, **10**, 855–867.
- NOBRE, C. A., SELLERS, P. S., and SHUKLA, J., 1991, Amazonia deforestation and regional climate change. *Journal of Climate*, **4**, 957–988.
- OLSON, J. S., 1992, World Ecosystems (WE1-4): Digital raster data on a 10-minute geographic 1080 × 2160 grid. *Global Ecosystems Database, Version 1-0: Disc A. Boulder, CO*, 3 independent single-attribute spatial layers on CD-ROM, 5 MB. National Geophysical Data Center, Washington, DC.
- PENNER, J. E., DICKINSON, R. E., and O'NEILL, C. A., 1992, Effects of aerosol from biomass burning on the global radiation budget. *Science*, **256**, 1432–1433.
- POTTER, G. L., ELSAESSER, H. W., MACCRACKEN, M. C., and LUTHER, F. M., 1975, Possible climatic impact of human deforestation. *Nature*, **258**, 697–698.
- PRINS, E. M., and MENZEL, W. P., 1994, Trends in South American biomass burning detected with the GOES visible infrared spin scan radiometer atmospheric sounder from 1983–1991. *Journal of Geophysical Research*, **99**, 16719–16735.
- RAMANATHAN, V., and COLLINS, W., 1991, Thermodynamic regulation of ocean warming by cirrus cloud deduced from observations of the 1987 El Niño. *Nature*, **351**, 27–32.
- RAO, C. R. N., ed., 1993, Degradation of the visible and near-infrared channels of the Advanced Very High Resolution Radiometer on the NOAA-9 spacecraft: assessment and recommendations for corrections. NOAA Technical Report NESDIS 70.
- RAO, C. R. N., SULLIVAN, J. T., WALTON, C. C., BROWN, J. W., and EVANS, R. H., 1993, Nonlinearity corrections for the thermal infrared channels of the Advanced Very High Resolution Radiometer: assessment and recommendations. NOAA Technical Report NESDIS 69.
- ROSBOROUGH, G. W., BALDWIN, D. G., and EMERY, W. J., 1994, Precise AVHRR image navigation. *IEEE Transactions on Geoscience & Remote Sensing*, **32**, 644–657.
- SALATI, E., and VOSE, P., 1983, Depletion of tropical rain forests, *Ambio*, **12**, 67–71.
- SCHWALLER, M., PRICE, R., and DALTON, J., 1993, Science data plan for the EOS data and information system covering EOSDIS version 0 and beyond. Version 2.0, NASA Goddard Space Flight Center, Greenbelt, MD.
- SHUKLA, J., NOBRE, C., and SELLERS, P., 1990, Amazon deforestation and climate change. *Science*, **247**, 1322–1325.
- SKOLE, D., and TUCKER, C., 1993, Tropical deforestation and habitat fragmentation in the Amazon: satellite data from 1978 to 1988, *Science*, **260**, 1905–1910.
- STEINWAND, D. R., 1994, Mapping raster imagery to the Interrupted Goode Homolosine Projection. *International Journal of Remote Sensing*, **15**, 3463–3471.
- STOWE, L. L., MCCLAIN, E. P., CAREY, R., PELLEGRINO, P., GUTMAN, G., DAVIS, P., LONG, C., and HART, S., 1991, Global distribution of cloud cover derived from NOAA/AVHRR operational satellite data. *Advances in Space Research*, **11**, 51–54.
- SUTTLES, J. T., GREEN, R. N., MINNIS, P., SMITH, G. L., STAYLOR, W. F., WIELICKI, B. A., WALKER, I. J., YOUNG, D. F., TAYLOR, V. R., and STOWE, L. L., 1988, Angular radiation models for earth-atmosphere system. Shortwave radiation, Vol. I, NASA Ref. Publ. 1184.
- SUTTLES, J. T., GREEN, R. N., SMITH, G. L., WIELICKI, B. A., WALKER, I. J., TAYLOR, V. R.,

- and STOWE, L. L., 1989, Angular radiation models for Earth-atmosphere system. Vol. 2, longwave radiation. NASA Reference Publication 1184.
- TOVINKERE, V. R., PENALOZA, M., LOGAR, A., LEE, J., WEGER, R. C., BERENDES, T. A., and WELCH, R. M., 1993, An intercomparison of artificial intelligence approaches for polar scene identification. *Journal of Geophysical Research*, **98**, 5001–5016.
- TOWNSHEND, J. R. G., 1994, Global data sets for land applications from the Advanced Very High Resolution Radiometer. *International Journal of Remote Sensing*, **15**, 3319–3332.
- UHL, C., BUSCHBACHER, R., and SERRAO, E. A. S., 1988, Abandoned pastures in eastern Amazonia. I: Patterns of plant succession. *Journal of Ecology*, **76**, 663–681.
- WARD, D. E., SUSOTT, R., KAUFFMAN, J., BABITT, R., HOLBEN, B. N., KAUFMAN, Y. J., SETZER, A., RASMUSSEN, R., CUMMING, D., and DIAS, B., 1992, Emissions and burning characteristics of biomass fires for cerrado and tropical rain forest regions of Brazil-BASE B experiment. *Journal of Geophysical Research*, **97**, 14601–14619.
- WELCH, R. M., SENGUPTA, S. K., and CHEN, D. W., 1988a, Cloud field classification based upon high spatial resolution textural features. Part I: Gray level concurrence matrix approach. *Journal of Geophysical Research*, **93**, 12663–12681.
- WELCH, R. M., SENGUPTA, S. K., and KUO, K. S., 1988b, Marine stratocumulus cloud fields off the coast of southern California observed using Landsat imagery. Part II: Textural analysis. *Journal of Applied Meteorology*, **27**, 362–378.
- WIELICKI, B. A., and GREEN, R. N., 1989, Cloud identification for ERBE radiative flux retrieval. *Journal of Applied Meteorology*, **28**, 1133–1146.